Molecular Simulation

ISSN: (Print) (Online) Journal homepage: www.tandfonline.com/journals/gmos20

Predicting optimal chain lengths in atomistic simulations of solvated polymers

Feranmi V. Olowookere & C. Heath Turner

To cite this article: Feranmi V. Olowookere & C. Heath Turner (2024) Predicting optimal chain lengths in atomistic simulations of solvated polymers, Molecular Simulation, 50:11, 687-695, DOI: 10.1080/08927022.2024.2341964

To link to this article: https://doi.org/10.1080/08927022.2024.2341964

MOLECULAR SIMULATION
2024, VOL. 50, NO. 11, 687–695
https://doi.org/10.1080/08927022.2024.2341964

Taylor & Francis
Taylor & Francis Group

Predicting optimal chain lengths in atomistic simulations of solvated polymers

Feranmi V. Olowookere and C. Heath Turner

Department of Chemical and Biological Engineering, The University of Alabama, Tuscaloosa, AL, USA

ABSTRACT

Currently, clear guidance is not available for determining the minimum practical chain lengths needed for achieving reasonable convergence when performing atomistic simulations of common synthetic polymers. Here, we analyze a collection of polymers, including polypropylene (PP), polyethylene naphthalate (PEN), polyethylene terephthalate (PET), polyethylene glycol (PEG), poly(methyl methacrylate) (PMMA), polystyrene (PS), and polyvinyl chloride (PVC), with chain lengths varying from 5 to 240 repeat units. We exclusively focus on solvated polymer systems, and we report the convergence of several characteristic properties, such as radial distribution functions (RDFs), surface area per repeat unit (SASA/N), ratio of mean squared end-to-end distance to mean squared radius of gyration ($\frac{\langle R^2 \rangle}{\langle R_g^2 \rangle}$), and surface electrostatic potential distributions. Based on these data, we propose a general relationship for identifying minimum practical chain lengths for performing atomistic simulations of solvated linear synthetic polymers, which is based on the SASA/N.

ARTICLE HISTORY
Received 1 February 2024
Accepted 5 April 2024

KEYWORDS
Chain length; atomistic simulations; upcycling; molecular dynamics

1. Introduction

It can be particularly difficult to extract consistent and reproducible polymer properties from a simulation, due to the complex interactions, structures, and correlated motions of these materials. Furthermore, the multiscale nature of polymers often requires advanced simulation techniques to establish consistent thermophysical properties of these materials [1–3]. While various theoretical approaches [1,4–7] and coarse-grained simulations [8–10] can provide significant improvements in computational efficiency, classical atomistic simulations still serve as the definitive benchmark for capturing molecular-scale phenomena in polymers [11]. With significant advancements in computational power, it is now possible to capture the atomistic behaviour of large synthetic polymers using molecular simulations, providing detailed insights into polymer structures, interactions, and dynamics [11–14]. However, a major challenge in conducting these simulations is maintaining a consistent modelling framework and accurately representing the long-chain polymer behaviour with a finite size atomistic model [11]. While chain-length dependencies can never be completely avoided, [1,15–17] achieving a balance between model size (i.e. chain length) and computational cost is an inherent consideration of all atomistic modelling studies involving polymers.

Selecting an appropriate chain length in a polymer-solvent model is still largely an area of speculation [18–21], with very little methodical investigation into this practical aspect. This issue has become even more urgent, given the increasing need to develop upcycling strategies for end-of-life plastics. In order to evaluate different polymer processing technologies (e.g. direct chemical modifications, new eco-friendly solvents, or the development of new composite materials) [22–24], it is essential to have reliable guidance for performing atomistic simulations of solvated polymer systems.

Historically, both structural (e.g. mean square end-to-end distance $\langle R^2 \rangle$) and dynamic properties (e.g. entanglement relaxation time, diffusion) of polymers pose complex theoretical challenges due to their dependence on chain length and molecular weight distribution, and are often simplified using generic polymer models in studies of power-law relationships [25–28]. A common example is the Kuhn model, which illustrates a polymer as a series of straight, rigid segments connected by flexible joints, and described by the equation $\langle R^2 \rangle = Nl^2$, where N is the number of repeat units and l is the length of a Kuhn segment [29]. Effects of chain length on these properties have also been extensively explored in all-atom Molecular Dynamics (MD) simulations for over two decades [30–33]. Interestingly, some of these studies suggest a threshold chain length where certain structural parameters become relatively constant, indicating a transition from small molecule to polymer-like behaviour. For instance, the Flory characteristic ratio for polystyrene (PS) in cyclohexane stabilises around $n \sim 10^3$ (where n is the number of main chain bonds), [28] similar to the consistent specific volume $v = 1.25$ cm^3/g observed at mean chain length $\bar{X} > 400$ in linear polyethylene (PE) melt models [30], and the diminishing first peak of the intermolecular pair distribution function in longer chain systems (C_{400} – C_{500}) [18,30]. The solubility parameter of a single atactic PS chain in toluene was also found to converge at $N \sim 50$ in an all-atom MD simulation study by Rasouli et al. [34]. Additionally, ring PE melts exhibit density stability at $N \sim 10^2$ repeat units in the asymptotic regime [33]. Ding

CONTACT C. Heath Turner hturner@eng.ua.edu
Supplemental data for this article can be accessed online at https://doi.org/10.1080/08927022.2024.2341964.

et al.'s experimental study [35] also highlights a transition in poly(dimethyl siloxane) (PDMS) and PS from small molecular behaviour to Rouse dynamics (when the chains begin to display Gaussian behaviour), with glass transition temperature (T_g) and density levelling off at a molecular weight of $M \sim$ 100,000 g/mol.

As we are exclusively focused on solvated polymer systems, we propose defining the optimal chain length for atomistic simulations as the minimal chain length at which polymer-solvent interactions do not significantly depend on the polymer chain length. In our investigation, we are less focused on the theoretical polymer physics. Rather, we are interested in establishing practical guidance and convergence metrics for reliably capturing polymer-solvent interactions in all-atom MD simulations (i.e. a balance between computational efficiency and accuracy), with the intent of achieving more consistency in future simulation studies.

In an initial exploration of this phenomenon [12], we examined the effects of polyvinyl chloride (PVC) chain length on its structure and dynamics in all-atom MD simulations. Our findings concluded that PVC_{120} (i.e. 120 PVC repeat units) can sufficiently represent the long-chain atomistic behaviour of PVC; the PVC_{120} model has been subsequently used to characterise its interactions with additives in traditional and bioderived solvents [36]. Our current work builds upon those findings by methodically exploring the chain-length dependence of a much broader set of other common synthetic polymers (PP, PEN, PET, PEG, PMMA, PS – see Figure 1) in order to establish a consistent framework for modelling dilute, solvated polymers in all-atom MD simulations.

2. Method

The MD simulations were performed using Gromacs 2021.1 [37]. We investigated seven distinct polymers, including PVC (as shown in Figure 1), with chain lengths ranging from 5 to 240 repeat units (refer to Table 1 for system compositions), using their most common respective experimental solvents [38–44]. Our objective is not to compare the different solvent performance (since the solvents differ). Rather, our primary goal is to independently maximise the polymer relaxation to accurately understand their properties when relaxed; snapshots of the PEG-H2O system are illustrated in Figure 2 and other snapshots can found in Figure S1. Unless stated, all PVC data is taken from our prior study, and we employ the same protocols to execute and process the simulations in the current work (so that direct comparisons can be made) [12].

The system configurations were initially minimised using the steepest descent method, followed by an annealing process. This involved heating each system to 800 K in the NVT ensemble, then cooling to 323 K over 25 ns. Subsequently, pressure was increased to 100 bar in the NPT ensemble and reduced to 1 bar in another 25 ns. This was followed by a 50 ns equilibration stage in the NPT ensemble, utilising the velocity rescaling thermostat [45] and Parrinello-Rahman barostat [46] to maintain constant pressure and temperature, a method validated in our previous studies [12,15,36] for decorrelating the end-to-end vectors of the polymer chain. A 50 ns production run was conducted to compute kinetic and thermodynamic properties, with data collected every 30 ps and statistical uncertainties determined through 5 ns block-averaging. All simulated data correspond to a temperature of 323 K and a pressure of 1 bar. It is also important to note that sufficiently large boxes and multiple replicas were employed for each system to avoid artificial correlations and to sufficiently explore phase space, so that the essential physics of the polymer-solvent model are reliably captured [47–49]. As such, the averaged properties and error bars were further calculated using a 95% confidence integral from three independent runs for each system.

The OPLS-AA force field [50] was used to describe the bonded and non-bonded interactions of the polymer and solvent molecules, and the atomic charges were obtained using the 1.14*CM1A-LBCC method [51]. The dispersion interactions were truncated with a 1.0 nm cut-off, and long-range electrostatic interactions were calculated using the Particle Mesh Ewald method [52]. The LINCS algorithm [53] constrained hydrogen bond lengths, with periodic boundary conditions applied in all dimensions.

The mean squared end-to-end distance ($\langle R^2 \rangle$) and radius of gyration ($\langle R_g^2 \rangle$)were obtained using the coordinates of the polymer chain as defined below:

$$\langle R^2 \rangle = \sum_{i=1}^{n} \langle (r_i)^2 \rangle \tag{1}$$

$$\left\langle R_g^2 \right\rangle = \frac{1}{2N^2} \sum_{n,m} \langle (r_n - r_m)^2 \rangle \tag{2}$$

Where r_n represents the coordinates of the n repeat units ($n = 1 \ldots N$) along the polymer chain, r_m is the center-of-mass of the polymer, and r_i is the distance between the carbon sites of the head and tail of the polymer. The shape descriptors, which include asphericity ($\langle b \rangle$), acylindricity ($\langle c \rangle$), and anisotropy ($\langle k \rangle$) are obtained from the average principal moments of $\langle R^2 \rangle$ (λ_x, λ_y, λ_z) using the PLUMED package [54] and are defined below:

$$\langle b \rangle = \frac{3}{2}\lambda_z^2 - \frac{\left\langle R_g^2 \right\rangle}{2} \tag{3}$$

$$\langle c \rangle = \lambda_y^2 - \lambda_z^2 \tag{4}$$

$$\langle k \rangle = \frac{3}{2} \frac{\lambda_x^4 + \lambda_y^4 + \lambda_z^4}{(\lambda_x^2 + \lambda_y^2 + \lambda_z^2)^2} - \frac{1}{2} \tag{5}$$

The criteria utilised to characterise a hydrogen bond (H-bond) is a maximum distance between donor and acceptor atoms of 3.5 Å and a maximum donor-hydrogen-acceptor angle of 35° [55]. The H-bond lifetime is quantified by calculating the autocorrelation function:

$$\langle P(t) \rangle = \frac{\langle s_{ij}(t_0) s_{ij}(t+\tau) \rangle}{\langle s_{ij}(t_0)^2 \rangle} \tag{6}$$

In which s_{ij} is 1 if there is a H-bond present and 0 otherwise. The H-bond lifetime τ_{HB} is obtained by fitting $P(t)$ to an

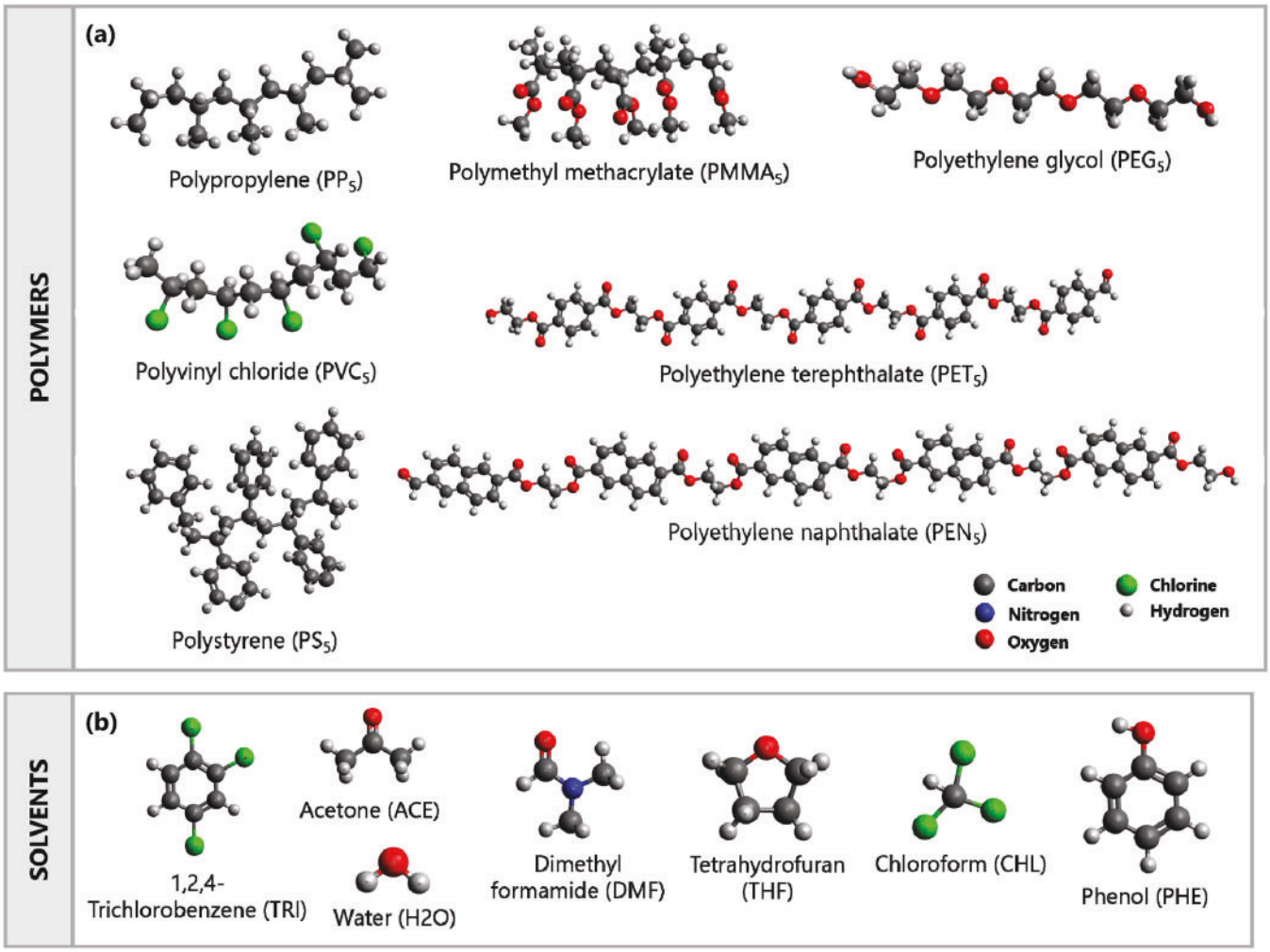

Figure 1. Molecular structures of the (a) polymers and (b) solvents. The polymer-solvent systems considered in this study are PEG-H2O, PEN-PHE, PET-CHL, PMMA-ACE, PP-TRI, PS-DMF and PVC-THF.

exponential function:

$$P(t) = \sum_i a_i \exp(-b_i t) \tag{7}$$

Where a_i and b_i are fitting parameters. Then, τ_{HB} is calculated as:

$$\tau_{HB} = \int_0^\infty P(t)\mathrm{d}t \tag{8}$$

Table 1. Number of solvent molecules for each polymer-solvent system. All systems correspond to 10% w/w polymer except PP-TRI (5% w/w PP). For each system, one polymer chain is present (see Figure 2).

No. of repeat units	PEG-H2O	PEN-PHE	PET-CHL	PMMA-ACE	PP-TRI	PS-DMF	PVC-THF
5	251	92	145	172	23	142	40
20	928	368	578	690	93	570	156
40	1875	736	1156	1379	186	1140	312
60	2803	1104	1734	2069	279	1710	470
100	4659	1840	2890	3448	464	2839	783
120	5587	2208	3468	4138	557	3454	940
240	10227	4416	6936	8276	1114	6908	1880

3. Results and discussion

In Tables S1 – S6, we present the average simulated densities, mean squared end-to-end distances ($\langle R^2 \rangle$), and the mean squared radii of gyration ($\langle R_g^2 \rangle$) of the studied polymers. With increasing number of repeat units, the densities of each polymer-solvent system tend to converge close to the longest polymer systems studied ($N = 240$). Figure 3(a) illustrates $\frac{\langle R^2 \rangle}{\langle R_g^2 \rangle}$ of the aforementioned solvated polymers versus the number of repeat units (N), with power law models (dashed lines) fitting the data points. As N increases, the $\frac{\langle R^2 \rangle}{\langle R_g^2 \rangle}$ values for all polymers gradually decline, reaching a point of convergence. Beyond a certain chain length, the ratio stabilises around 0.5–2 which is considerably smaller than for a freely-jointed chain model (~ 6) [56]. On the other hand, this behaviour is more consistent with that of the self-avoiding walk model described by the Flory theory [57], which is typically less than 6 and accounts for volume exclusion of polymers in good solvents. Furthermore, it also implies that $\langle R^2 \rangle$ and $\langle R_g^2 \rangle$ may continue to scale proportionally with increasing

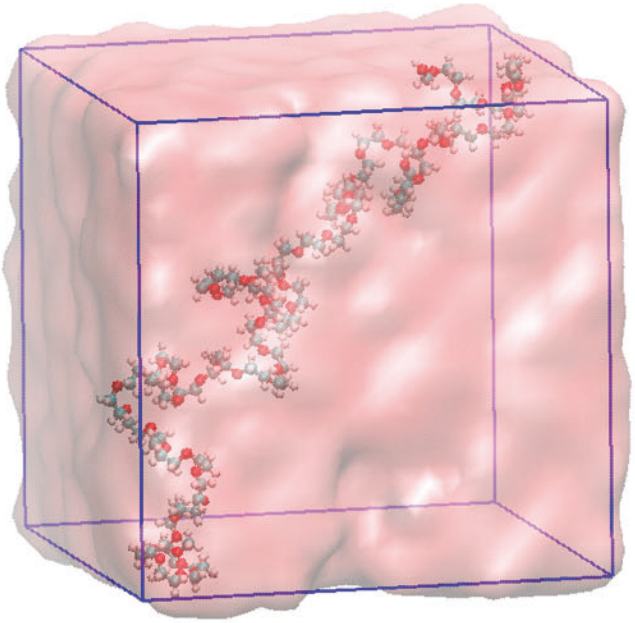

Figure 2. Visual snapshots of the PEG-H2O system. The transparent regions represent the solvent molecules while the bold solid spheres represent the atoms of the polymer chain (cyan = carbon, red = oxygen, white = hydrogen). Snapshots of other systems can be found in Figure S1.

chain length, similar to previous polymer simulation studies [58–60].

Figure 3(b–d) present the average asphericity $\langle b \rangle$ and acylindricity $\langle c \rangle$ normalised by $\langle R_g^2 \rangle$, along with the average relative anisotropy $\langle k \rangle$, as a function of N of the studied polymers. As N increases, there is a general decrease in both $\frac{\langle b \rangle}{\langle R_g^2 \rangle}$ and $\frac{\langle c \rangle}{\langle R_g^2 \rangle}$ values, indicating that chains become less spherical and cylindrical with larger N. Rutledge [61] explains this as short-range intramolecular forces dominating in shorter chains, leading them to display rod-like characteristics in segments. Similar to the $\frac{\langle R^2 \rangle}{\langle R_g^2 \rangle}$ ratio, these values tend to stabilise for longer chains ($N \sim 120$), showing diminishing change with respect to N. This is consistent with studies by Theodorou and Suter [62] which also describe this convergence of shape parameters as limiting values for polymer chains. Additionally, $\langle k \rangle$ increases with increasing N, but its dependence on N is less pronounced than that of $\langle b \rangle$ and $\langle c \rangle$. For some polymers (e.g. PVC and PS), $\langle k \rangle$ values show a relatively constant trend with increasing N.

Complementing this, Figure 4 shows that as N increases, the solvent accessible surface area per N (SASA/N) values decrease and eventually converge to consistent values. PET and PEN have higher SASA/N values compared to PEG, PVC, and PP across the different chain lengths. The results agree with theoretical insights, particularly from the Flory-Huggins framework [59], which addresses the energetics of polymer-solvent interactions (suggesting that as N approaches infinity, the system approaches a thermodynamic limit). Here, adding more monomers minimally affects the polymer solution, resulting in a more uniform surface area exposure when normalised by N. Dimitriyev and co-workers [63] also noted this phenomenon, emphasising that in such a limit, the translational entropy of polymers becomes negligible relative to the solvent's entropy, particularly for sufficiently long polymers.

Next, we calculate the number of H-bonds (N_{HB}) between PEG and H2O. The scaling relationship between N_{HB}/N and N is illustrated in Figure 5(a). As N increases, fluctuations exist around a mean value of $N_{HB}/N \sim 0.7$ from $N = 5$ to $N = 100$. A noticeable jump in N_{HB}/N is then observed when transitioning from 100 ($N_{HB}/N \sim 0.7$) to 120 repeat units ($N_{HB}/N \sim 1.1$), and subsequently stabilises. This step around $N = 120$, particularly when considered with the SASA/N results could suggest stabilisation in the hydrogen bonding. The H-bond autocorrelation function ($P(\tau)$) in Figure 5(b) supports this, showing increasing $P(\tau)$ with N and a plateau in H-bond lifetime (shown in the inset plot) around $N = 120$ ($N = 160$ was also included to help confirm the convergence trend). The convergence of the H-bond behaviour at $N = 120$ across both figures suggests a transition in the hydrogen bonding network in the system at this chain size.

To help quantify the convergence of the polymer-solvent interactions across the different systems, we analyze the site-to-site radial distribution functions (RDFs) between the polymers and solvents, as depicted in Figure S2. Subsequently, Figure 6 presents a composite summary of the maximum g(r) values of the first peak versus N to elucidate the changes in the intensity of interactions between the polymer and solvent (similar plots for other RDFs are presented in Figure S3). As N increases, the peak intensity for all polymer-solvent systems, represented by the g(r) maximum, diminishes. The $g(r)$ for $N = 5$ is the highest, but the intensity decreases monotonically with increasing N, indicating a relative weakening between the solvent-polymer interactions beyond a minimal polymer length; this is likely due to the ability of the polymer to increasingly interact with itself beyond $N = 5$. Eventually, distinct convergence points emerge for each of these polymers. For instance, PET tends to converge around $N = 20$, while PS does so around $N = 60$. This is consistent with the SASA/N results, which show that the polymer achieves a consistent surface exposure to the solvent per repeat unit, and the interactions remain stable as N continues to increase. Increasing N not only reduces the g(r) maximum to a consistent value, but other RDF features (in Figure S2) also seem to adopt a consistent pattern, suggesting that beyond a certain chain length, adding more repeat units does not significantly alter the polymer's structural behaviour or its interactions with the surrounding solvent molecules. In a study to estimate the chemical potential in atomistic polymer systems, Yamada et al. [64] also highlighted that the RDF deviations between a solute polymer chain (with incremental monomer index i) and surrounding solvent molecules become diminished at $i = 100$ (compared to $i = 40$ and 60), suggesting a converged interaction of the tagged polymer with surrounding molecules. This enables the calculation of a chain length-insensitive averaged free energy of a chain increment.

We also evaluate the average surface electrostatic potential (ESP) of these polymers in solution. The electrostatic potential distribution for PMMA is presented in Figure 7, as a

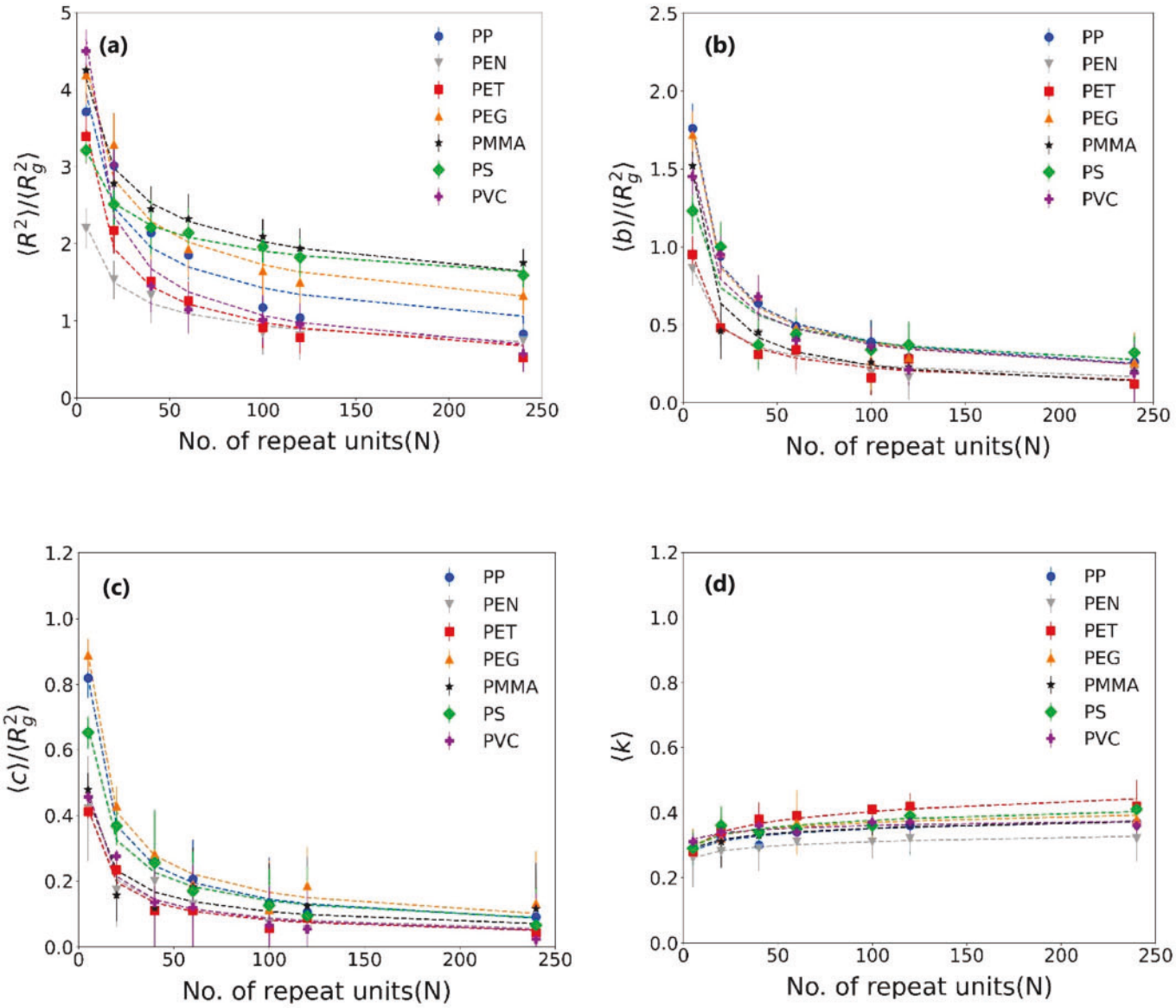

Figure 3. Repeat unit dependence of different configurational properties for PP, PEN, PET, PEG, PMMA, PS and PVC in their respective solvents: (a) $\frac{\langle R^2 \rangle}{\langle R_g^2 \rangle}$, (b) average relative asphericity $\langle b \rangle / \langle R_g^2 \rangle$ and (c) average relative acylindricity $\langle c \rangle / \langle R_g^2 \rangle$, and (d) average anisotropy $\langle k \rangle$. Power law models (dashed lines) are used to fit the data points. PVC data is taken from the literature [12].

representative example, while the distributions for the remaining polymers are illustrated in Figure S4. We observe that as N increases, the ESP distribution slightly broadens (centred around zero), and the distributions become more consistent, with fewer outliers (e.g. in PP). The peak heights also tend to decrease as N increases. This ESP behaviour suggests that longer polymer chains present a more statistically representative electrostatic surface topography, with a more consistent distribution of charged and non-charged regions interfacing with the surrounding solvent.

Our simulation analyses of several different synthetic polymer chain lengths enable us to provide more quantitative guidance for determining the balance between accuracy and computational efficiency in atomistic simulations of solvated polymers. While most of the above computed properties (e.g. electrostatic potential, shape descriptors) demonstrate good convergence with respect to N, there is some inherent variability; the convergence trends are not completely monotonic across the various polymer systems. However, among the different system characteristics, the RDFs appear to be the most predictable and sensitive measure for quantifying relative convergence. Therefore, we propose a surrogate criterion (RDF convergence) as a practical guide for determining solvated polymer convergence with respect to the number of monomer repeat units of the polymer model:

$$\text{Deviation } \% = \frac{1}{N_{r,\text{points}}} \sum_{j}^{N_{r,\text{points}}} \frac{g_i(r) - g_{240}(r)}{g_{240}(r)} \times 100 \qquad (9)$$

where $g_i(r)$ is the RDF for the system with i repeat units and $N_{r,\text{points}}$ denotes the total number of discrete distances (r) where $g(r)$ is calculated, with each distance being separated by a bin width of 0.05 nm. A numerical threshold of 2% defines when the RDF has sufficiently converged (see Table S7). In Figure 8,

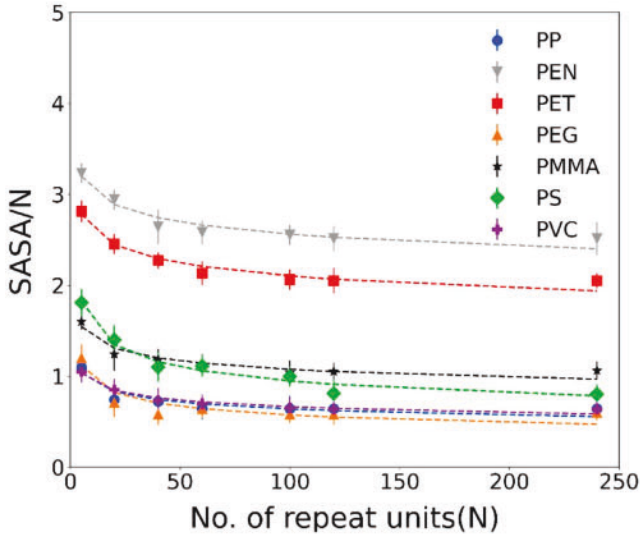

Figure 4. Repeat unit dependence of SASA/N for PP, PEN, PET, PEG, PMMA, PS and PVC in their respective solvents. Data points are fitted using power law models, indicated by dashed lines.

we plot ln(N) (where N is the minimum number of repeat units required to achieve RDF convergence) versus the SASA/N of the longest polymer models ($N = 240$) to establish a more general guide for determining optimal polymer chain lengths for these (and potentially other) atomistic polymers in solution. The graph indicates a decrease in required N to reach convergence as the value of SASA/N increases. We could group these polymers in two distinct sections on the graph. The first group, comprised of PEG, PVC, PP, PS, and PMMA, corresponds to a higher value of N and a lower SASA/N value, while the second group, PET and PEN corresponds to a smaller N and a higher SASA/N value. The data stretches from around 0.5 nm^2 to 2.50 nm^2 in SASA/N, which is a broad range of normalised surface area values; other synthetic polymers (not tested here) would also likely fit within this range, and thus, the correlation could serve as simulation design guidance.

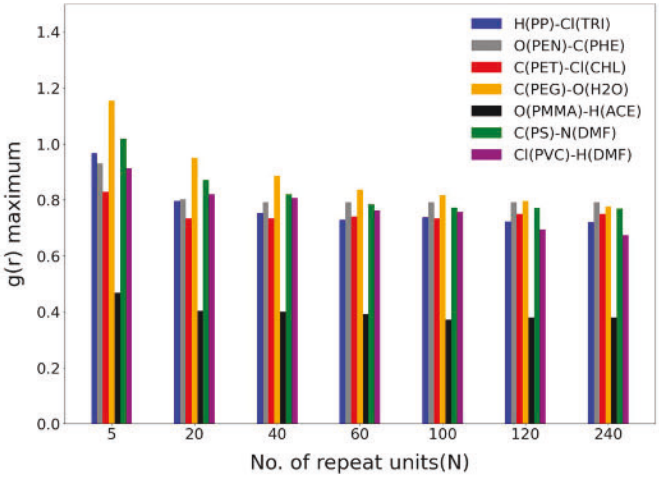

Figure 6. First peak maxima of the g(r) values from the polymer-solvent RDFs in Figure S2 as a function of the number of polymer repeat units.

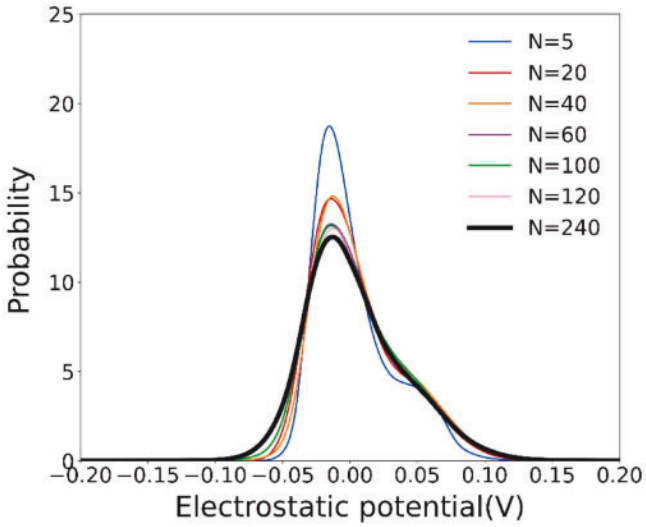

Figure 7. Average surface ESP distribution of the PMMA polymer in the ACE solvent.

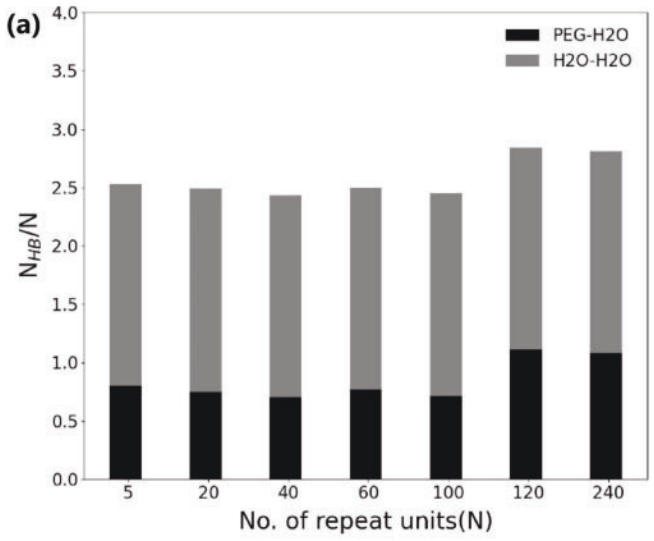

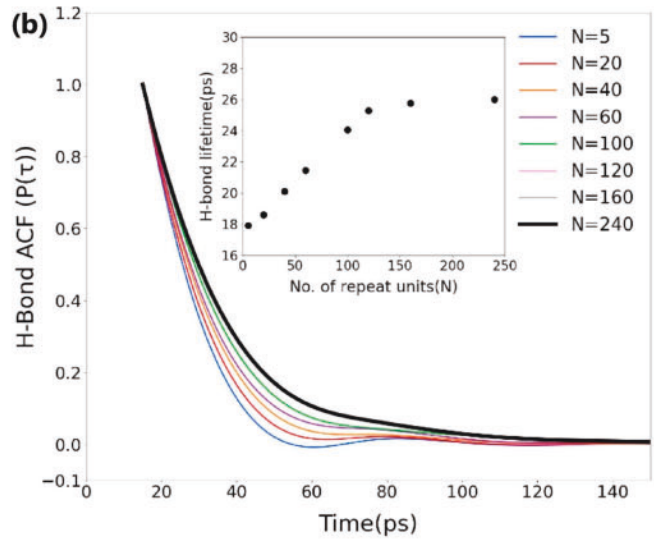

Figure 5. (a) Number of H-bonds per repeat unit and (b) H-bond autocorrelation function of PEG in H2O; the inset shows the corresponding average H-bond lifetime.

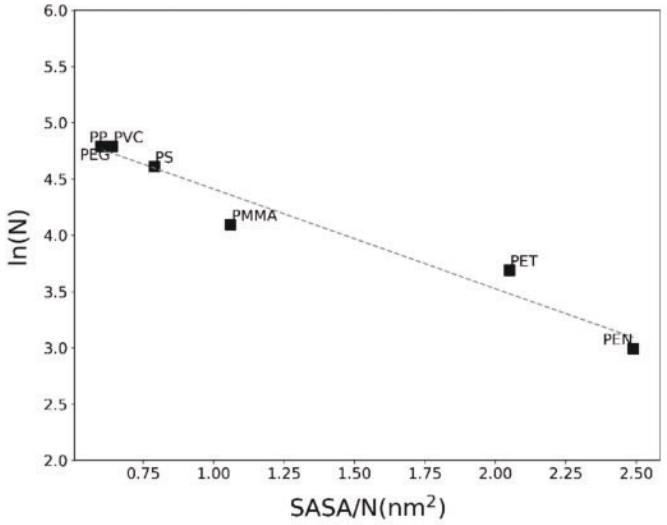

Figure 8. ln(N) versus SASA/N required to achieve our RDF convergence criterion (<2%) defined in equation (9).

4. Conclusions

Herein, all-atom MD simulations are used to study the effects of chain lengths on conformational properties of various polymers in solvents to develop a useful framework for predicting optimal chain lengths in atomistic polymer simulations. Our analyses of several different synthetic polymers suggest that surface area estimates could be a potential predictor for determining the optimal chain lengths. The inverse correlation between repeat units and SASA/N highlights that polymers with larger repeat unit surface areas (e.g. PET, PEN) require shorter chain lengths for reliable simulations. It is fundamentally important to recognise that the finite-chain-length corrections are unavoidable in polymer systems, implying that their dynamics will never fully converge, as evidenced in previous studies [1,16,17]. The magnitude of these corrections varies depending on the specific system under study, such as whether to account for entanglements or the concentration level involved. Nonetheless, our analyses should help guide others in identifying an appropriate polymer model which reliably captures the fundamental polymer-solvent interactions, without needlessly overextending computational resources. This should be particularly useful when using all-atom MD simulations to screen the performance of alternative solvents for common synthetic polymers.

Acknowledgements

We are grateful to the Alabama Supercomputer Authority for computational support.

Disclosure statement

No potential conflict of interest was reported by the author(s).

Funding

This work is supported by the National Science Foundation (Award Nos. 2132133 and 2029387).

Availability of data and materials

The datasets generated during and/or analyzed during the current study are available from the corresponding author on reasonable request.

References

[1] Everaers R, Karimi-Varzaneh HA, Fleck F, et al. Kremer–Grest models for commodity polymer melts: linking theory, experiment, and simulation at the Kuhn scale. Macromolecules. 2020;53(6):1901–1916. doi:10.1021/acs.macromol.9b02428

[2] Hollborn K-U, Schneider L, Müller M. Effect of slip-spring parameters on the dynamics and rheology of soft, coarse-grained polymer models. J Phys Chem B. 2022;126:6725–6739. doi:10.1021/acs.jpcb.2c03983

[3] Li W, Jana PK, Behbahani AF, et al. Dynamics of long entangled polyisoprene melts via multiscale modeling. Macromolecules. 2021;54(18):8693–8713. doi:10.1021/acs.macromol.1c01376

[4] Young N, Balsara N. Flory–Huggins equation. In: Kobayashi S, Müllen K, editors. Encyclopedia of polymeric nanomaterials. Berlin, Heidelberg: Springer; 2014. p. 1–7.

[5] Liu J-L, Li C-L. A generalized Debye-Hückel theory of electrolyte solutions. AIP Advances. 2019;9:015214. doi:10.1063/1.5081863

[6] Venkatram S, Kim C, Chandrasekaran A, et al. Critical assessment of the Hildebrand and Hansen solubility parameters for polymers. J Chem Inf Model. 2019;59:4188–4194. doi:10.1021/acs.jcim.9b00656

[7] Cohen SR, Alshareedah I, Borcherds WM, et al. Modified Rouse-Zimm theory for computing sequence-specific viscoelastic properties of biomolecular condensates. Biophys J. 2023;122:206a. doi:10.1016/j.bpj.2022.11.1238

[8] Nguyen D, Tao L, Li Y. Integration of machine learning and coarse-grained molecular simulations for polymer materials: physical understandings and molecular design. Front Chem. 2022;9:820417. doi:10.3389/fchem.2021.820417

[9] Dhamankar S, Webb MA. Chemically specific coarse-graining of polymers: methods and prospects. J Polym Sci. 2021;59:2613–2643. doi:10.1002/pol.20210555

[10] Joshi SY, Deshmukh SA. A review of advancements in coarse-grained molecular dynamics simulations. Mol Simul. 2021;47:786–803. doi:10.1080/08927022.2020.1828583

[11] Gartner III TE, Jayaraman A. Modeling and simulations of polymers: a roadmap. Macromolecules. 2019;52(3):755–786. doi:10.1021/acs.macromol.8b01836

[12] Olowookere FV, Al Alshaikh A, Bara JE, et al. Effects of chain length on the structure and dynamics of polyvinyl chloride during atomistic molecular dynamics simulations. Mol Simul. 2023;49(15):1401–1412. doi:10.1080/08927022.2023.2234493

[13] Zhang Z, Wang Y, Liu P, et al. Quantitatively predicting the mechanical behavior of elastomers via fully atomistic molecular dynamics simulation. Polymer. 2021;223:123704. doi:10.1016/j.polymer.2021.123704

[14] Kumar A, Sharma K, Dixit AR. A review on the mechanical and thermal properties of graphene and graphene-based polymer nanocomposites: understanding of modelling and MD simulation. Mol Simul. 2020;46:136–154. doi:10.1080/08927022.2019.1680844

[15] Olowookere FV, Barbosa GD, Turner CH. Coarse-grained molecular dynamics modeling of polyvinyl chloride: solvent interactions, mechanical behavior, and dehydrochlorination effects. Macromolecules. 2023;56(24):10006–10015. doi:10.1021/acs.macromol.3c02211

[16] Dünweg B, Kremer K. Molecular dynamics simulation of a polymer chain in solution. J Chem Phys. 1993;99:6983–6997. doi:10.1063/1.465445

[17] Bormuth A, Henritzi P, Vogel M. Chain-length dependence of the segmental relaxation in polymer melts: molecular dynamics simulation studies on poly (propylene oxide). Macromolecules. 2010;43:8985–8992. doi:10.1021/ma101721d

[18] Harmandaris VA, Mavrantzas VG, Theodorou DN. Atomistic molecular dynamics simulation of polydisperse linear polyethylene

melts. Macromolecules. 1998;31:7934–7943. doi:10.1021/ma980698p
[19] Zou L, Zhang W. Molecular dynamics simulations of the effects of entanglement on polymer crystal nucleation. Macromolecules. 2022;55:4899–4906. doi:10.1021/acs.macromol.2c00817
[20] Zuo B, Zhou H, Davis MJ, et al. Effect of local chain conformation in adsorbed nanolayers on confined polymer molecular mobility. Phys Rev Lett. 2019;122:217801. doi:10.1103/PhysRevLett.122.217801
[21] Cai X, Liang C, Liu H, et al. Conformation and structure of ring polymers in semidilute solutions: a molecular dynamics simulation study. Polymer. 2022;253:124953. doi:10.1016/j.polymer.2022.124953
[22] Wojnowska-Baryła I, Bernat K, Zaborowska M. Plastic waste degradation in landfill conditions: the problem with microplastics, and their direct and indirect environmental effects. Int J Environ Res Public Health. 2022;19:13223. doi:10.3390/ijerph192013223
[23] Jung H, Shin G, Kwak H, et al. Review of polymer technologies for improving the recycling and upcycling efficiency of plastic waste. Chemosphere. 2023;320:138089. doi:10.1016/j.chemosphere.2023.138089
[24] Wang C, Han H, Wu Y, et al. Nanocatalyzed upcycling of the plastic wastes for a circular economy. Coord Chem Rev. 2022;458:214422. doi:10.1016/j.ccr.2022.214422
[25] Clisby N. Accurate estimate of the critical exponent ν for self-avoiding walks via a fast implementation of the pivot algorithm. Phys Rev Lett. 2010;104:055702. doi:10.1103/PhysRevLett.104.055702
[26] Clisby N, Dünweg B., High-precision estimate of the hydrodynamic radius for self-avoiding walks. Phys Rev E. 2016;94:052102. doi:10.1103/PhysRevE.94.052102
[27] Shirvanyants D, Panyukov S, Liao Q, et al. Long-range correlations in a polymer chain due to its connectivity. Macromolecules. 2008;41:1475–1485. doi:10.1021/ma071443r
[28] Wittmer J, Meyer H, Baschnagel J, et al. Long range bond-bond correlations in dense polymer solutions. Phys Rev Lett. 2004;93:147801. doi:10.1103/PhysRevLett.93.147801
[29] Doi M, Edwards SF. The theory of polymer dynamics. Oxford: Clarendon; 1988. p. 10–12.
[30] Mavrantzas VG, Boone TD, Zervopoulou E, et al. End-bridging Monte Carlo: a fast algorithm for atomistic simulation of condensed phases of long polymer chains. Macromolecules. 1999;32:5072–5096. doi:10.1021/ma981745g
[31] Doxastakis M, Mavrantzas V, Theodorou D. Atomistic Monte Carlo simulation of cis-1, 4 polyisoprene melts. I. Single temperature end-bridging Monte Carlo simulations. J Chem Phys. 2001;115:11339–11351. doi:10.1063/1.1416490
[32] Gestoso P, Nicol E, Doxastakis M, et al. Atomistic Monte Carlo simulation of polybutadiene isomers: cis-1, 4-polybutadiene and 1, 2-polybutadiene. Macromolecules. 2003;36:6925–6938. doi:10.1021/ma034033l
[33] Ramos J, Vega JF, Martínez-Salazar J. Predicting experimental results for polyethylene by computer simulation. Eur Polym J. 2018;99:298–331. doi:10.1016/j.eurpolymj.2017.12.027
[34] Rasouli S, Moghbeli MR, Nikkhah SJ. A comprehensive molecular dynamics study of a single polystyrene chain in a good solvent. Current Applied Physics. 2018;18:68–78. doi:10.1016/j.cap.2017.10.010
[35] Ding Y, Kisliuk A, Sokolov A. When does a molecule become a polymer? Macromolecules. 2004;37:161–166. doi:10.1021/ma035618i
[36] Olowookere FV, Barbosa GD, Turner CH. Characterizing polyvinyl chloride interactions with additives in traditional and bioderived solvents. Ind Eng Chem Res. 2024;63:1109–1121. doi:10.1021/acs.iecr.3c03809
[37] Abraham MJ, Murtola T, Schulz R, et al. GROMACS: high performance molecular simulations through multi-level parallelism from laptops to supercomputers. SoftwareX. 2015;1:19–25. doi:10.1016/j.softx.2015.06.001
[38] Ensing B, Tiwari A, Tros M, et al. On the origin of the extremely different solubilities of polyethers in water. Nat Commun. 2019;10:2893. doi:10.1038/s41467-019-10783-z
[39] Mourey T, Slater L, Galipo R, et al. Size-exclusion chromatography of poly (ethylene 2, 6-naphthalate). J Chromatogr A. 2012;1256:129–135. doi:10.1016/j.chroma.2012.07.067
[40] Demir T, Wei L, Nitta N, et al. Toward a long-chain perfluoroalkyl replacement: water and oil repellency of polyethylene terephthalate (PET) films modified with perfluoropolyether-based polyesters. ACS Appl Mater Interfaces. 2017;9:24318–24330. doi:10.1021/acsami.7b05799
[41] Slobodian P, Lengálová A, Sáha P, et al. Poly (methyl methacrylate)/multi-wall carbon nanotubes composites prepared by solvent cast technique: composites electrical percolation threshold. J Reinf Plast Compos. 2007;26:1705–1712. doi:10.1177/0731684407081437
[42] Mori S, Barth HG, Mori S, et al. High-temperature size exclusion chromatography. Berlin: Springer; 1999. p. 156–164.
[43] Toy PH. Polystyrene. In: Charette A, Bode J, Rovis T, et al., editors. Encyclopedia of Reagents for Organic Synthesis (EROS). Hoboken: Wiley; 2005. p. 56–57.
[44] Blackley DC. Synthetic rubbers: their chemistry and technology: their chemistry and technology. New York: Springer Science & Business Media; 2012. p. 87–89.
[45] Bussi G, Donadio D, Parrinello M. Canonical sampling through velocity rescaling. J Chem Phys. 2007;126:014101. doi:10.1063/1.2408420
[46] Parrinello M, Rahman A. Polymorphic transitions in single crystals: a new molecular dynamics method. J Appl Phys. 1981;52:7182–7190. doi:10.1063/1.328693
[47] Mo J, Wang J, Wang Z, et al. Size and dynamics of a tracer ring polymer embedded in a linear polymer chain melt matrix. Macromolecules. 2022;55:1505–1514. doi:10.1021/acs.macromol.1c02388
[48] Zifferer G. Monte Carlo simulation studies of the size and shape of linear and star-branched polymers embedded in the tetrahedral lattice. Macromol Theory Simul. 1999;8:433–462. doi:10.1002/(SICI)1521-3919(19990901)8:5<433::AID-MATS433>3.0.CO;2-C
[49] Gkolfi E, Bačová P, Harmandaris V. Size and shape characteristics of polystyrene and poly (ethylene oxide) star polymer melts studied by atomistic simulations. Macromol Theory Simul. 2021;30:2000067. doi:10.1002/mats.202000067
[50] Jorgensen WL, Maxwell DS, Tirado-Rives J. Development and testing of the OPLS all-atom force field on conformational energetics and properties of organic liquids. J Am Chem Soc. 1996;118:11225–11236. doi:10.1021/ja9621760
[51] Dodda LS, Vilseck JZ, Tirado-Rives J, et al. 1.14* CM1A-LBCC: localized bond-charge corrected CM1A charges for condensed-phase simulations. J Phys Chem B. 2017;121:3864–3870. doi:10.1021/acs.jpcb.7b00272
[52] Darden T, York D, Pedersen L. Particle mesh Ewald: an N· log (N) method for Ewald sums in large systems. J Chem Phys. 1993;98:10089–10092. doi:10.1063/1.464397
[53] Hess B, Bekker H, Berendsen HJ, et al. LINCS: a linear constraint solver for molecular simulations. J Comput Chem. 1997;18:1463–1472. doi:10.1002/(SICI)1096-987X(199709)18:12<1463::AID-JCC4>3.0.CO;2-H
[54] Tribello GA, Bonomi M, Branduardi D, et al. PLUMED 2: new feathers for an old bird. Comput Phys Commun. 2014;185:604–613. doi:10.1016/j.cpc.2013.09.018
[55] Weng L, Stott SL, Toner M. Molecular dynamics at the interface between ice and poly(vinyl alcohol) and ice recrystallization inhibition. Langmuir. 2018;34:5116–5123. doi:10.1021/acs.langmuir.7b03243
[56] Flory PJ, Volkenstein M. Statistical mechanics of chain molecules. New York: Wiley Online Library; 1969.
[57] Bhattacharjee SM, Giacometti A, Maritan A. Flory theory for polymers. J Phys: Condens Matter. 2013;25:503101. doi:10.1088/0953-8984/25/50/503101

[58] Nyambura CW, Sampath J, Nance E, et al. Exploring structure and dynamics of the polylactic-co-glycolic acid–polyethylene glycol copolymer and its homopolymer constituents in various solvents using all-atom molecular dynamics. J Appl Polym Sci. 2022;139:e52732. doi:10.1002/app.52732

[59] Sherck N, Webber T, Brown DR, et al. End-to-end distance probability distributions of dilute poly (ethylene oxide) in aqueous solution. J Am Chem Soc. 2020;142:19631–19641. doi:10.1021/jacs.0c08709

[60] Tow GM, Maginn EJ. Fully atomistic molecular dynamics simulations of hydroxyl-terminated polybutadiene with insights into hydroxyl aggregation. Macromolecules. 2020;53:2594–2605. doi:10.1021/acs.macromol.9b02632

[61] Rutledge G. Rotational isomeric state approach to the single-chain behavior of aromatic polyesters. Macromolecules. 1992;25:3984–3995. doi:10.1021/ma00041a022

[62] Theodorou DN, Suter UW. Shape of unperturbed linear polymers: polypropylene. Macromolecules. 1985;18:1206–1214. doi:10.1021/ma00148a028

[63] Dimitriyev MS, Chang Y-W, Goldbart PM, et al., Swelling thermodynamics and phase transitions of polymer gels. Nano Futures. 2019;3:042001. doi:10.1088/2399-1984/ab45d5

[64] Yamada K, Matubayasi N. Chain-increment method for free-energy computation of a polymer with all-atom molecular simulations. Macromolecules. 2020;53:775–788. doi:10.1021/acs.macromol.9b01952